# Electron densities, temperatures, and the dielectric function of femtosecond-laser-produced plasmas

W. Theobald, R. Häßner, R. Kingham,* and R. Sauerbrey
*Institut für Optik und Quantenelektronik, Friedrich-Schiller-Universität Jena, Max-Wien-Platz 1, D-07743 Jena, Germany*

R. Fehr, D. O. Gericke, M. Schlanges, and W.-D. Kraeft
*Institut für Physik, Universität Greifswald, Domstr.10a, 17487 Greifswald, Germany*

K. Ishikawa
*Institut für Theoretische Physik A, RWTH Aachen, 52056 Aachen, Germany*
(Received 17 July 1998; revised manuscript received 19 October 1998)

The optical properties of dense plasmas in the extreme ultraviolet spectral range are investigated experimentally and theoretically. A method is presented that enables measurement of electron densities in excess of $10^{24}$ cm$^{-3}$. High-order harmonics are transmitted through a femtosecond-laser-produced plasma probing the optical density at several wavelengths. This technique has the advantage of providing direct access to ultrahigh electron densities, and achieves a precision of about 20% at zero time delay. The dielectric function of a dense carbon plasma was calculated including effects of higher density and the contribution of bound electrons. [S1063-651X(99)05703-7]

PACS number(s): 52.25.Mq, 52.25.Fi, 52.40.Nk

## I. INTRODUCTION

The interaction of high intensity femtosecond laser pulses with matter allows the production of plasmas with high electron densities and short scale lengths. Much work has concentrated on the generation and characterization of ultrashort x-ray bursts [1], on investigations of the plasma dynamics [2–4] and on transport properties of dense plasmas through reflectivity measurements [5–9]. Production of matter in such a state allows the study of basic plasma physics in regimes relevant to astrophysics, atomic physics, or in strongly correlated plasmas [10–12].

There are few experimental methods to study the evolution of femtosecond-laser-produced plasmas, and up to now only time-resolved x-ray spectroscopy could reveal substantial information [3,4]. We have demonstrated an experimental method that uses high harmonics produced by intense laser radiation to probe the evolution of ultrashort laser-produced plasmas [13]. Differential absorption of the harmonics allows the measurement of plasma electron densities well above the critical density of the fundamental wavelength. It is shown that this pump-probe technique gives direct access to ultrahigh electron densities and electron temperatures in conjunction with a time resolution on the order of the laser pulse duration. In order to investigate whether high density effects become important for the interpretation of the measurements, theoretical studies of the dielectric function of a dense carbon plasma were performed. The calculations show that the standard Drude model is a good approximation even for high density plasmas.

*On leave from Plasma Physics Group, Imperial College, London SW7 2BZ, U.K.

## II. EXPERIMENTAL INVESTIGATIONS

The principle of the experiment which probes the optical properties of a dense plasma is shown in Fig. 1. The idea is to measure the transmittance of a plasma at two or more frequencies in such a way that some of them are below the plasma frequency while others are above. Light can only propagate in a plasma with an electron density $n_e < n_c$, where $n_c$ is the critical density given by

$$n_c = (4\pi^2 \varepsilon_0 m_e c^2)/(e^2 \lambda^2) \approx 1.11 \times 10^{21}/(\lambda/\mu\mathrm{m})^2 \ \mathrm{cm}^{-3}.$$

Since typical electron densities in plasmas produced by femtosecond laser-solid interaction are $\sim 10^{23}$ cm$^{-3}$ and the temporal evolution occurs on a subpicosecond time scale, ultrashort extreme ultraviolet (xuv)-pulses must be used to probe these plasmas. A convenient way to produce an xuv-spectrum of distinct frequencies is high-order harmonic generation in a gas jet [14]. Depending on $n_e$, high-order harmonics are transmitted through the femtosecond-laser-

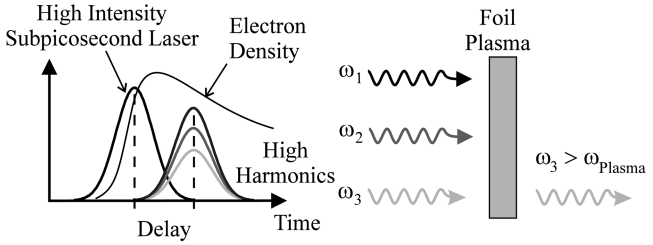


FIG. 1. Principle of the method. A high intensity subpicosecond laser pulse creates a dense plasma in a thin foil which is subsequently irradiated by temporally correlated high harmonics after a certain delay time. Depending on the density, higher order harmonics are better transmitted than lower order harmonics, and from the measured ratio of the transmitted signal the electron density can be deduced.

 

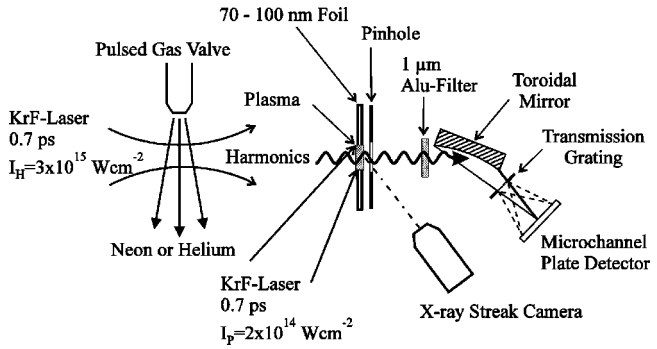


FIG. 2. Experimental setup. From the left hand side high-order harmonics created in an inert gas jet pass through a plasma that was generated by a temporally correlated subpicosecond laser pulse in a thin polycarbonate foil. A pinhole after the foil restricts the transmitted radiation subsequently detected by a soft-x-ray spectrograph. An x-ray streak camera is used to align the temporal overlap of the two laser pulses.

produced plasma, while lower-order harmonics are absorbed or reflected. The electron density is then inferred from the measured ratio of the transmitted harmonics. By measuring the opacity of the plasma at various evolution stages, both $n_e$ and the electron temperature $T_e$ can be mapped out in time.

### A. Experimental setup

We used a short-pulse hybrid dye–KrF laser system which provided 0.7-ps, 40-mJ laser pulses at a wavelength of 248.5 nm with a 1-Hz repetition rate [15,16]. The experiment took place in a vacuum vessel of 1-m diameter evacuated to a pressure of $\sim 10^{-5}$ mbar. Figure 2 depicts the experimental setup. The *p*-polarized laser beam was divided into two parts, with one beam of 10-mJ pulse energy focused to an intensity between $2\times10^{14}$ and $7\times10^{14}$ W/cm$^2$ onto a 70–100-nm-thick polycarbonate foil target (Lexan 101, GE Plastics) in order to generate a dense plasma. The laser spot diameter was measured with a microscope, and was varied between 50 and 100 $\mu$m. The second temporally correlated laser pulse with 30-mJ pulse energy was focused into an inert gas jet, and reached an intensity of $\sim 3\times10^{15}$ W/cm$^2$. High-order harmonics were produced down to a wavelength of 19.2 nm (13th harmonic of a KrF laser), which acted as a probe beam. Harmonics beyond the 13th order could not be observed due to a 1-$\mu$m thick aluminum filter in front of the spectrograph. The *L* edges of aluminum are at 17 and 14.3 nm, respectively. In our case the fifth and seventh harmonics of the KrF radiation at 49.7 and 35.5 nm were intense enough to be used.

Preplasma formation was not observed because the contrast ratio in the experiment was better than $10^7$. The contrast is defined as the ratio of peak pulse power to that of the pedestal before the main pulse. A simple experimental test was performed to confirm that no preplasma formation occurred. The frequency doubled femtosecond seed pulse emitted by the dye laser was blocked and only the amplified spontaneous emission (ASE) of the excimer amplifiers was focused onto the foil target. No damage of the foil was observed with an ASE intensity of $\sim 10^7$ W/cm$^2$. If a seed pulse had been allowed to pass through the amplifiers, the content of the ASE energy would have been even lower for our hybrid dye-excimer laser system due to gain depletion [16].

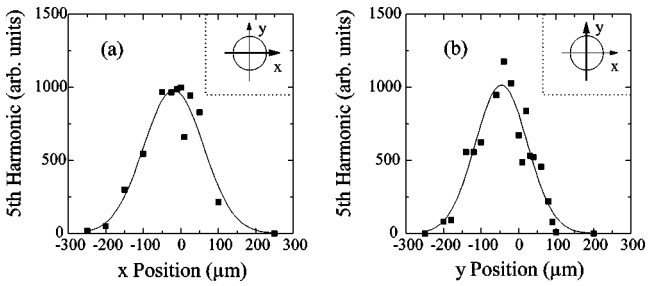


FIG. 3. Spatial measurement of the fifth harmonic intensity observed through a 50-$\mu$m pinhole which was located at the target plane instead of the foil. The pinhole was shifted in two perpendicular directions in the target plane.

A piezoelectric drive pulsed valve was used to release a gas jet with a particle density of about $3\times10^{17}$ cm$^{-3}$. The foil target was located 8 mm behind the gas nozzle, and the laser beam which created the high-order harmonics illuminated an area of $700\times600$ $\mu$m$^2$ on the foil. This gave an intensity of $\sim 10^{13}$ W/cm$^2$ of the fundamental on the foil, but the area which was illuminated by harmonics was smaller. Figure 3 shows a measurement of the fifth harmonic beam spatial profile in two perpendicular directions in the target plane. For this measurement, the foil target was replaced by a pinhole of 50-$\mu$m diameter which could be shifted in the target plane. Curve (*a*) was measured in the *x* direction, and has a $1/e^2$ radius of $w_x=160$ $\mu$m. In the y direction a value of $w_y=140$ $\mu$m is obtained. In general, the radius of a harmonic with order *q* should be smaller than that of the fundamental [17], which is in agreement with the observed values. Typical energy conversion efficiencies for high harmonics are between $\sim 10^{-6}$ to $\sim 10^{-7}$, resulting in a probe intensity of $\sim 10^8-10^7$ W/cm$^2$ for the fifth harmonic. The temporal duration is estimated to be less than 300 fs based on blueshift measurements of the third harmonic of the KrF-laser radiation [18]. Only linear absorption of the harmonics in the plasma is considered at these intensities. The linear absorption coefficient of Lexan increases from 35 up to 65 $\mu$m$^{-1}$ in the wavelength region between 35 and 50 nm [19]. Therefore the transmittance in the xuv spectral range decreases from 3% to 0.2% in a 100-nm-thick foil, and the Lexan strongly attenuates the harmonics. A pinhole of 200-$\mu$m diameter was located 300 $\mu$m behind the foil to restrict the area from which the transmitted radiation was detected.

After the foil burns through, the expected maximum electron density is $\sim 10^{23}$ cm$^{-3}$, while at later times hydrodynamic expansion and recombination will eventually lead to a decay of $n_e$. The plasma was irradiated by the harmonics at various time delays, which could be adjusted with a precision of about 60 fs by a delay line in one of the beam paths. The zero time delay coarse alignment was performed by an x-ray streak camera to within $\pm 2$ ps. This was refined by the pump-probe measurement itself to a precision of about 0.5 ps, which is on the order of the pulse duration. A single shot soft-x-ray spectrograph with a spectral range from 2 to 70 nm was used for detecting the transmitted xuv radiation [20]. A toroidal mirror imaged the source 1:1 onto a microchannel

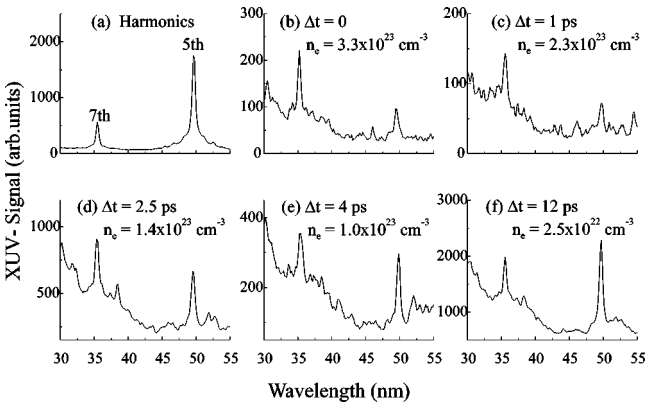


FIG. 4. Measured spectra of the fifth (49.7 nm) and seventh (35.5 nm) harmonics of a KrF laser which were transmitted at different pump-probe time delays through a subpicosecond laser-produced foil plasma. The harmonics were produced in a neon gas jet. In (a), part of the harmonic spectrum without a foil target is shown, while in (b)–(f) the spectra are shown when a dense plasma is present. The plasma was generated at a laser intensity of $2\times10^{14}$ W/cm$^2$ in a polycarbonate foil with a thickness of 100 nm. The electron density deduced from the intensity ratio of both harmonics is given in each figure.

plate detector which was coupled to a photodiode array. A free standing gold transmission grating (1000 lines per mm) acted as a dispersive element.

### B. Results

Figure 4 shows single shot transmitted spectra measured at various delay times up to 12 ps for a plasma generated at a laser intensity of $2\times10^{14}$ W/cm$^2$ from a 100-nm-thick foil. Without a foil target [Fig. 4(a)], i.e., at zero electron density, the fifth harmonic appears about three times more intense than the seventh harmonic when the harmonics are produced in neon gas. In Fig. 4(a), a pinhole of 50-$\mu$m diameter (which is comparable to the focal spot size) was placed in the target plane instead of a foil. This ensures that the signal can be compared to the signal transmitted through a plasma of similar size which is shown in Figs. 4(b)–4(f). In contrast to 4(a), when a dense plasma is present, the seventh harmonic is stronger than the fifth at zero delay (pump and probe overlap in time), as can be seen in Fig. 4(b). When the probe precedes the plasma creating pulse, only plasma self emission as a background at all delay times is observed. The intensity ratio of the transmitted seventh to fifth harmonics, $R_{7/5}$, gradually decreases with increasing time delay [Figs. 4(c)–4(f)] and reaches after several picoseconds the original ratio, indicating that both harmonics are transmitted equally. Qualitatively this series of spectra shows the expected behavior: in the case of a dense plasma [Fig. 4(b)], the higher frequency is transmitted more effectively than the lower frequency. The ratio gradually decreases while the plasma is freely expanding and recombining, which results in a decreasing electron density with time. For long times between the plasma creation and the probe radiation the original ratio is almost recovered since a sufficiently dilute plasma transmits both harmonics equally. The electron densities inferred from the intensity ratio are shown in each plot. This is explained in detail further below in Sec. II C. They range from $3.3\times10^{23}$ cm$^{-3}$ immediately after the plasma creation [Fig. 4(b)] to $2.5\times10^{22}$ cm$^{-3}$ after an expansion time of 12 ps [Fig. 4(f)].

### C. Analysis

As the harmonics pass through the foil plasma, three different absorption mechanisms must be considered, namely, bound-bound, bound-free, and free-free absorption. Each contribution has been estimated by assuming a plasma in local thermodynamic equilibrium (LTE). LTE is valid for quasihydrogenic $K$-shell ions when $n_e$ in cm$^{-3}$ is larger than $5\times10^{17}(Z^*)^6\sqrt{T_e/eV}$ for a given electron temperature $T_e$ and charge state $Z^*$ [21]. For typical values of $T_e=100$ eV and $Z^*=4$, the minimum electron density necessary for LTE to hold is $\sim2\times10^{22}$ cm$^{-3}$. Since the measured initial electron densities are larger than $10^{23}$ cm$^{-3}$, LTE is a valid approximation. The degree of ionization and the level population of each ion species were calculated with the Saha equation and the Boltzmann distribution respectively. The empirical sum formula for basic resin polycarbonate is $(C_{16}H_{14}O_3)_n$ which is the same for Lexan 101 (GE Plastics, MSDS Data sheet). In the following calculations for the absorption coefficients the concentration ratio C:H:O =16:14:3 was taken into account for the resulting plasma.

Absorption of the fifth harmonic at 49.7 nm due to bound-bound transitions in carbon can only arise from the $2p^2$-$2p3d$ ($\lambda=49.9$ nm) transition in C III and the $1s3p$-$1s5d$ ($\lambda=49.7$ nm) transition in C V. The seventh harmonic at 35.5 nm can be absorbed by the 3–5 transition ($\lambda=35.6$ nm) in C VI. In oxygen, the fifth harmonic can be absorbed by $2s^22p^3$-$2s^22p^2(^3P)4s$ ($\lambda=50.0$ nm) transitions in O II, and by $1s^23p$-$1s^24d$ ($\lambda=49.8$ nm) transitions in O VI. The wavelength of the seventh harmonic is in the wavelength range of the $2s2p^3$-$2s2p^2(^4P)3d$ ($\lambda=35.5-35.7$ nm) transitions in O III. It has to be taken into account that the ionization energy of ions in a dense plasma must be corrected with respect to their values in vacuum due to lowering of the continuum edge. Energy is released when electron-ion pairs are immersed in a plasma, leading to a reduction of the ionization energy which is quite substantial for solid density plasmas. The reduction of the ionization energy for an ion with charge state $Z$ for a Debye plasma is given by [22]

$$\Delta E_\infty=\frac{(Z+1)e^2}{4\pi\varepsilon_0\lambda_D}, \tag{2.1}$$

where $\lambda_D$ is the Debye radius. This formula estimates reductions of $\Delta E_\infty\approx(Z+1)\times9.3$ eV and $(Z+1)\times13.7$ eV for $T_e=150$ eV, $n_e=3.4\times10^{23}$ cm$^{-3}$ ($\lambda_D\approx1.6$ Å) and for $T_e=50$ eV, $n_e=2.5\times10^{23}$ cm$^{-3}$ ($\lambda_D\approx1.1$ Å), respectively. Hence, due to the large reduction of the continuum edge, the upper states of the above mentioned transitions are no longer bound, and all fall into the continuum. This means that bound-bound absorption does not have to be considered further.

A substantial contribution arises from bound-free absorption or photoionization. Actual photoionization cross sections for atoms and ions with $Z\leqslant30$ can be found in Refs. [23,24]. A good interpolation formula that fits the smoothed

contribution of each threshold energy $\nu_T$ to the photoionization cross section as a function of photon energy $\nu$ is [24]

$$\sigma_{\mathrm{bf}}(\nu)=\sigma_T\left[\beta\left(\frac{\nu}{\nu_T}\right)^{-s}+(1-\beta)\left(\frac{\nu}{\nu_T}\right)^{-s-1}\right], \quad \nu>\nu_T, \tag{2.2}$$

where $\sigma_T$ is the cross section at the threshold, and $\beta$ and $s$ are tabulated constants. The interpolation formula is a good approximation for photon energies within a few times the threshold energy. Typical values for the cross sections of the different carbon and oxygen ion species are on the order of $10^{-18}$ cm$^2$. Photoionization was calculated for each atomic shell $(K,L,M,\ldots)$ of the different carbon, hydrogen, and oxygen ions. Due to continuum lowering only the levels up to the highest bound state were taken into account. The cross sections were calculated using Eq. (2.2), assuming that the threshold $\nu_T$ is lowered according to Eq. (2.1). We calculate a maximal absorption coefficient of $\alpha_{\mathrm{bf}}\leqslant 4\times10^3$ cm$^{-1}$ for both harmonics in the case of a Lexan plasma with $n_{\mathrm{ion}}=0.94\times10^{23}$ cm$^{-3}$ and $T_e$ in the range of 50–150 eV which is relevant for our experiments. The mass density or specific gravity of Lexan 101 is 1.2 g/cm$^3$, resulting in an average ion particle density of $n_{\mathrm{ion}}=0.94\times10^{23}$ cm$^{-3}$. The absorption coefficients for photoionization are at least 25 times smaller than those for free-free absorption (i.e., inverse bremsstrahlung) which were calculated using the Drude model (see below) and are $\alpha_{\mathrm{ff}}(5)\approx3\times10^5$ cm$^{-1}$ and $\alpha_{\mathrm{ff}}(7)\approx1\times10^5$ cm$^{-1}$ for the fifth and seventh harmonics respectively at $n_e=3\times10^{23}$ cm$^{-3}$. Therefore, photoionization contributes less than 4% to the total absorption under the present conditions and only collisional heating is considered in the following analysis.

In order to extract both $n_e$ and $T_e$ from the measured spectra, the dependence of the refractive index on $n_e$ has to be known. For the data evaluation the standard Drude model is used to derive the plasma refractive index. The Drude model was further refined by taking higher correlation effects into account, which are relevant for high density, as described in Sec. III. The Fresnel formula is applied in order to describe the reflection of the harmonics assuming a steep density gradient plasma, which is justified in our case as discussed below. The probe radiation impinges perpendicular to the plasma surface and the fraction of the radiation that is reflected is given by $R=|(\eta-1)/(\eta+1)|^2$. The fraction $T$ of the radiation transmitted through a homogeneous plasma sheet of thickness $d$ with a boxlike electron density profile that is probed under normal incidence is

$$T=(1-R)^2e^{-\alpha d}, \tag{2.3}$$

taking into account back-reflection at the rear density step. Here only the linear absorption coefficient $\alpha=2(\omega/\mathrm{c})\,\eta_i$ for collisional absorption is utilized. If multiple beam interference is considered due to reflection at the rear and front density steps, the formula for the transmitted fraction $T$ becomes

$$T=\frac{(1-R)^2e^{-\alpha d}}{(1-\mathrm{Re}^{-\alpha d})^2+4\,\mathrm{Re}^{-\alpha d}\sin^2(\delta/2)}, \tag{2.4}$$

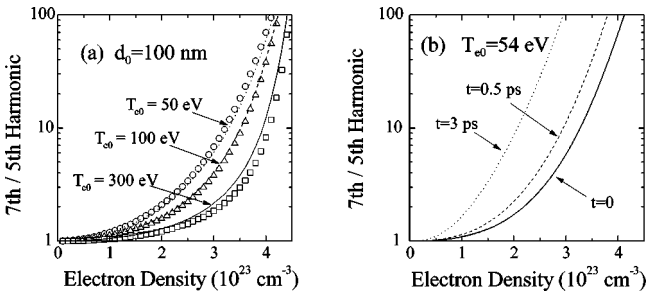


FIG. 5. (a) Calculation of the seventh to fifth harmonics transmitted ratio through a 100-nm foil plasma as a function of $n_e$ for various electron temperatures. The solid, dashed, and dotted curves were calculated by determining the degree of ionization with the Saha equation, while the open symbols are for a fixed charge state of 3.9. (b) The temporal evolution of the ratio for an initially 100-nm-thick plasma sheet with $T_{e0}=54$ eV.

where $\delta$ is a phase shift given by $\delta=2\pi(1+2\,\eta_r d/\lambda)$. The product $\mathrm{Re}^{-\alpha d}$ is small compared to unity, and never exceeds 0.02 and 0.01 for the fifth and seventh harmonics, respectively. Neglecting multiple beam interference, Eq. (2.3) is a valid approximation which results in an error of less than 5% for the deduced $n_e$.

Now we are in a position to calculate the transmitted signal of the seventh and fifth harmonics as a function of $n_e$. The curves in Fig. 5 show the ratio $R_{7/5}$ of the transmitted seventh and fifth harmonics (for various $T_e$ at 100-nm thickness) as a function of $n_e$ calculated assuming LTE. The Saha equation was solved for a carbon plasma in order to determine the degree of ionization for each temperature and density. In contrast, the open symbols were calculated assuming a fixed charge state of 3.9. As one can see, $R_{7/5}$ is not very sensitive to the degree of ionization. For a given ratio the electron density can be directly inferred from this graph. At zero delay a ratio [deduced from Fig. 4(b)] of $9.2^{+2.5}_{-3.1}$ was measured, which leads to an initial electron density between $n_{e0}=(3.2\pm0.2)\times10^{23}$ and $(3.9^{+0.1}_{-0.2})\times10^{23}$ cm$^{-3}$, assuming $T_e=50$ and 300 eV, respectively. The ratio depends only weakly on $T_e$. Although the simultaneous determination of both $n_e$ and $T_e$ using a *single* measurement is ambiguous, each can be uniquely determined by observing the time evolution of $R_{7/5}$. For a delay of -0.5 ps no harmonic contributions are detected, and therefore the plasma is produced between -0.5 ps and zero. The burn-through time for a 100-nm foil is estimated to be about 0.5 ps, which is calculated assuming an ionization front velocity of $1.8\times10^7$ cm/s [25] as measured for similar laser intensities and similar plasma conditions. The ionization time of the foil target is shorter than the presently used laser pulses (0.7 ps), but for shorter laser pulses it restricts the temporal resolution around zero time delay. This might be resolved by using thinner foils or producing a faster shock wave at a higher laser intensity, which helps to shorten the ionization time of the target.

After the foil burns through and the laser pulse ceases, it is assumed that the plasma undergoes an adiabatic expansion due to the lack of heat transport and negligible radiation cooling. To a good approximation the plasma expansion is uniform and planar at the two outer edges since the lateral plasma dimension (about 50 $\mu$m) is much larger than the thickness of the expanding plasma sheet. A constant expan-

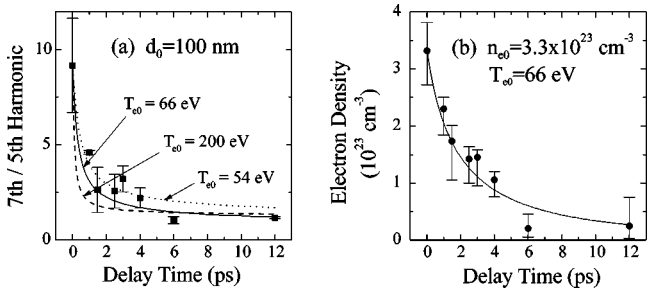


FIG. 6. (a) The measured ratios of the seventh to the fifth harmonics (solid squares), which were inferred from the spectra in Fig. 4, are shown as a function of the delay time. The dashed and dotted curves are calculations of the ratio assuming various initial electron temperatures without taking recombination into account. The solid curve is the best fit that takes recombination into account. (b) The evolution of $n_e$ inferred from (a) (solid dots) is shown together with a calculation for $T_{e0}=66$ eV (solid curve).

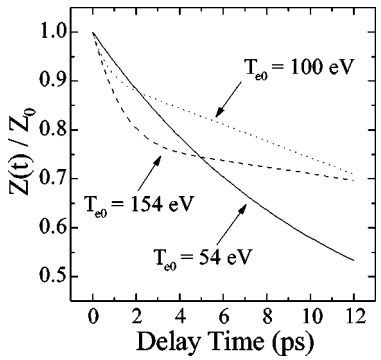


FIG. 7. Decay of the charge state normalized to the initial charge state due to recombination in an expanding carbon plasma. The curves are calculated for various initial temperatures. The Saha equation is solved for each time step.

sion at the ion sound velocity $c_s=\sqrt{(\langle Z\rangle k_B T_{e0})/M_{\rm ion}}$ is assumed, where $\langle Z\rangle$ is the degree of ionization, $T_{e0}$ is the initial electron temperature, and $M_{\rm ion}$ is an average ion mass taking into account the concentration of the different ion species in the Lexan target. For $\langle Z\rangle=3.4$ and $T_{e0}=54$ eV, a value of $c_s\approx 5\times 10^6$ cm/s is obtained, resulting in a plasma expansion of about 0.6 $\mu$m in 12 ps which is much smaller than the lateral plasma dimension of about 50 $\mu$m. The electron density decays with time like $n_e=n_{e0}(d_0/d)$, where $n_{e0}$ is the initial electron density, $d_0$ the initial thickness, and $d=d_0+c_s\Delta t$ the thickness for a time delay $\Delta t$. The electron temperature develops in time according to $T_e=T_{e0}(d_0/d)^{\gamma-1}$, where $\gamma=\frac{5}{3}$ is the adiabatic coefficient. In Fig. 5(b), $R_{7/5}$ is calculated using Eq. (2.3) for various time delays for an expanding plasma with $d_0=100$ nm and $T_{e0}=54$ eV. For increasing time delays the curves are constantly shifted to the left, which implies a decreasing density for a given measured ratio. Simulations of an expanding foil plasma were performed with the one-dimensional Lagrangian hydrodynamic code MEDUSA [26,27] in order to check the assumption of adiabatic expansion. For time delays up to 1.0 ps, the foil expansion modeled by MEDUSA is essentially adiabatic. By comparing the predicted maximum electron density from MEDUSA with that from the adiabatic expansion model above, we find that the electron density of the latter is accurate to within 20% in the first picosecond. For longer delay times (up to 5 ps) the electron density determined by adiabatic expansion tends to exceed the electron density predicted by MEDUSA. For delay times larger than 5 ps, the electron densities found from MEDUSA are about half of those given by pure adiabatic expansion. However, we will use the simple adiabatic expansion model for data evaluation, since it provides the possibility of a fit to the experimental data in contrast to using a hydrodynamic code. In addition, the fit which reveals the initial density and temperature is most sensitive within the first 2 ps when recombination is not significant. This justifies the use of the simple adiabatic expansion model.

Figure 6(a) shows $R_{7/5}$ (square symbols) extracted from the measurement (Fig. 4) as a function of time. The ratio at zero delay is initially $9.2^{+2.5}_{-3.1}$, and decreases with time to $1.2^{+0.1}_{-0.2}$ at 12 ps. The curves shown in Fig. 6(a) are calculations of the temporal evolution of the ratio for various initial electron temperatures. The dashed and dotted curves are calculations neglecting the effect of recombination. In that case the dotted curve with $T_{eo}=(54^{+41}_{-25})$ eV fits the measured values best resulting in an initial electron density of $n_{e0}=(3.2^{+0.5}_{-0.6})\times 10^{23}$ cm$^{-3}$ by using Fig. 5. In addition to the plasma expansion, recombination also results in a drop in $n_e$. The effect of recombination is considered here by estimating how the degree of ionization evolves for a carbon plasma using the Saha equation (see Fig. 7). For delay times in excess of $\sim 5$ ps, an additional decrease in $n_e$ by at most a factor of 2 is estimated. Figure 7 shows a calculation of the decreasing degree of ionization normalized to the initial charge state as a function of time for various $T_{e0}$. Plasma adiabatic expansion leads to cooling, and therefore to a decreasing charge state with time. The data were reanalyzed including the effect of recombination. The recalculated decay is shown as solid line in Fig. 6(a), and approaches the experimental values at later delay times more accurately. The best fit is obtained for a slightly higher initial temperature of $(66^{+50}_{-30})$ eV. Figure 6(b) shows the electron densities inferred from the experimental measurements (solid circles) versus time, together with the calculated decay. The deduced initial plasma parameters ($\Delta t=0$) are $n_{e0}=(3.3^{+0.5}_{-0.6})\times 10^{23}$ cm$^{-3}$ and $T_{e0}=(66^{+50}_{-30})$ eV. The thickness of the foil is known to within an accuracy of 10%, and results in an error of about 3% in the determination of $n_{eo}$.

As mentioned earlier, the Fresnel formula is applied in order to describe the partial reflection of the harmonic probe radiation at the vacuum plasma interfaces. It turns out that under the present conditions the transmitted probe radiation intensity is controlled by absorption, and the exact shape of electron density profile is not important for the reflectivity. Figure 8(a) shows the reflected (solid curve) and the absorbed (dashed) fraction of the incident fifth harmonic through a dense carbon plasma of thickness 70 nm as a function of $n_e$. At the critical density of the fifth harmonic of $4.5\times 10^{23}$ cm$^{-3}$, the reflectivity reaches a value of 30%. As expected, the transmissivity of the foil plasma, which is shown in Fig. 8(b), decreases with increasing $n_e$. A calculation that includes reflection (solid curve) gives a slightly lower transmissivity than the calculation that takes only absorption into account (dashed curve). The error one would

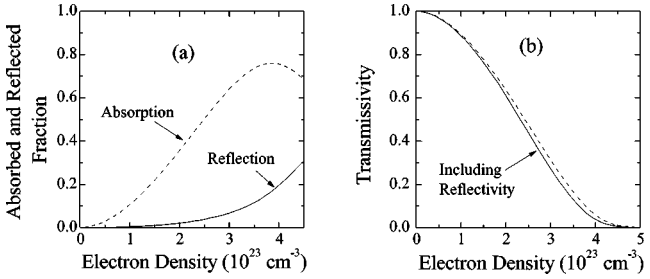


FIG. 8. (a) Absorbed and reflected fractions of the fifth harmonic radiation transmitted through a 70-nm carbon plasma layer with $T_{e0}=150$ eV and an average degree of ionization of 5.2. (b) The transmissivity of the fifth harmonic as a function of $n_e$ including reflection (solid curve), and by taking only absorption into account (dashed curve).

make by determining the density from the dashed curve instead of the solid curve, i.e., ignoring reflection, is about 5% over the whole density range. The assumption of a steep plasma gradient is therefore not critical for the quantitative results.

More important for the determination of the plasma density is refraction of the harmonics in a steep lateral density gradient, which is shown schematically in Fig. 9. High harmonics are incident from the left hand side onto a foil plasma with a radial electron density gradient at the boundary to unionized foil material. This causes a gradient in the refractive index which tends to bend the xuv radiation into the direction of the gradient. The refraction angle is smaller for shorter wavelengths, and therefore this might influence the measured ratio of the seventh to the fifth harmonics. Qualitatively this effect is negligible for small transverse scale lengths $L$ because the annular area in which refraction occurs is small compared to the focal area. On the other hand, for large transverse scale lengths the index gradient becomes small, and consequently refraction decreases again. A more detailed description of the calculation is found in the Appendix. Refraction of the harmonic radiation in the plasma due to a lateral density gradient has to be considered for radial scale lengths shorter than 10 $\mu$m. The relative refraction losses $(1-x_7)/(1-x_5)$ (see the Appendix) stay below 1.2 for all scale lengths which means that the loss of the fifth harmonic is at most 20% higher than for the seventh harmonic, which is almost completely collected by the spectrograph for each scale length. This was taken into account in the uncertainty of the determined $n_e$. Density fluctuations in the central part of the distribution are expected not to be critical, since even for gradients of up to $3\times10^{26}$ cm$^{-4}$ the radiation is always in the acceptance angle of the spectrograph.

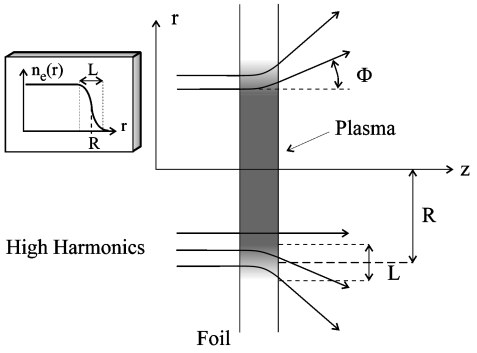


FIG. 9. Schematic of the refraction of high harmonics in a lateral electron density profile $n_e(r)$ of a foil plasma. The inset on the left hand side qualitatively shows the decrease of $n_e$ with radius $r$. In the steepest part of the density gradient, considerable refraction of the harmonics occurs upon propagation through the plasma sheet.

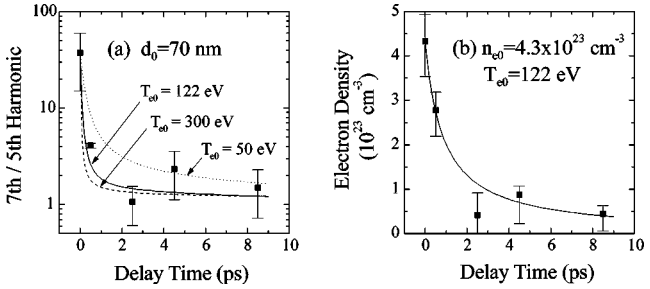


FIG. 10. (a) The measured ratio of the seventh to the fifth harmonics (solid squares) versus delay time for a plasma that was generated in a 70-nm-thick foil at a laser intensity of $5\times10^{14}$ W/cm$^2$. The curves are calculations for the time dependence of the ratio for various initial electron temperatures. For the dotted and dashed curves recombination was neglected, while the solid curve is the best fit taking recombination into account. (b) The evolution of $n_e$ inferred from (a) (solid squares) is shown together with a calculation for $T_{e0}=122$ eV (solid curve).

### D. Second and third experiments

In a second experiment the plasma was generated in a 70-nm foil with a laser intensity of about $5\times10^{14}$ W/cm$^2$, yielding the initial parameters of $n_{e0}=(4.3^{+0.6}_{-0.8})\times10^{23}$ cm$^{-3}$ and $T_{e0}=(122^{+92}_{-56})$ eV. Figure 10(a) shows the measured and calculated ratios as functions of the delay time, and Fig. 10(b) shows the extracted density decay with time. The faster decay of $R_{7/5}$ indicates a higher $T_{e0}$, which is consistent with the higher degree of ionization. Recombination was not considered for the dotted and dashed curves, while the solid curve is the best fit and takes recombination into account. It should be emphasized that the time evolution of $R_{7/5}$ is only a function of $n_{e0}$ and $T_{e0}$. These two parameters are directly obtained from the measurement.

Figure 11 shows a sequence of measured spectra obtained in a third experiment, where a helium rather than a neon gas jet was used. Spectra of harmonics transmitted through a plasma produced in a 100-nm Lexan foil at a laser intensity of $2\times10^{14}$ W/cm$^2$ are displayed for various delay times. The fifth and seventh harmonics generated in the helium gas jet [Fig. 11(a)] now appear to be equal in strength without a foil target. Qualitatively the same behavior is observed as in Fig. 4, and the extracted ratios are displayed in Fig. 12 as a function of time showing the evolution of the plasma. The deduced initial conditions are $T_{e0}=(61^{+46}_{-28})$ eV and $n_{e0}=(3.2^{+0.5}_{-0.6})\times10^{23}$ cm$^{-3}$.

The measured values for $n_e$ obtained from all three measurements at zero time delay are between 23% and 35% higher than the values which were calculated using the Saha equation. The measured maximum electron density is $n_{e0}=(4.3^{+0.6}_{-0.8})\times10^{23}$ cm$^{-3}$, and appears to be slightly higher than the $n_e=3.8\times10^{23}$ cm$^{-3}$ that is calculated for a fully

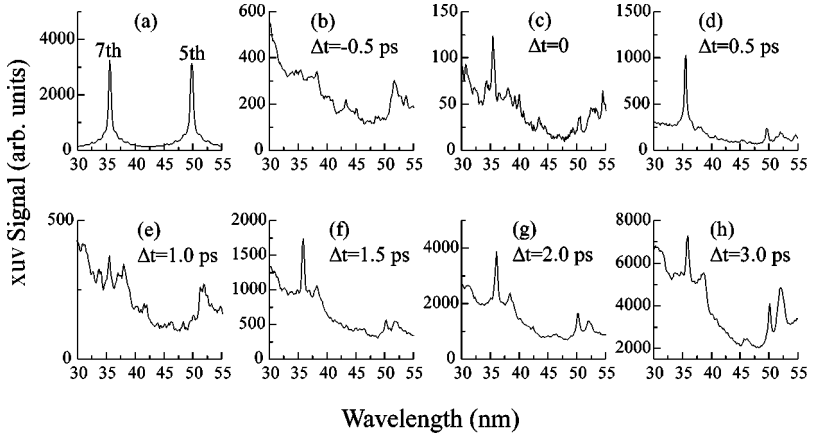


FIG. 11. Spectra of the fifth (49.7 nm) and seventh (35.5 nm) harmonics of a KrF laser transmitted at different pump-probe time delays through a subpicosecond-laser-produced plasma. The plasma was generated at a laser intensity of $2\times10^{14}$ W/cm$^2$ in a foil with a thickness of 100 nm. The harmonics were produced in a helium gas jet.

ionized but unexpanded foil. A possible explanation might be that a shock front during the laser interaction leads to a local increase of the density, and therefore higher electron densities are measured at zero delay time. This is confirmed by simulations using MEDUSA, which show that during the laser interaction time a shock wave leads to electron densities of up to $5\times10^{23}$ cm$^{-3}$ for the laser parameters which were used in the experiments.

### III. OPTICAL PROPERTIES OF DENSE PLASMAS

The experiments with the KrF laser at intensities around $10^{14}$ W/cm$^2$ have shown that a high density plasma with a moderate electron temperature is produced. Such a plasma enters the regime of strong coupling, and hence femtosecond-laser-produced plasmas are well suited to study this interesting range. Usually, the plasma parameter $\Gamma=1/(n_e\lambda_D^3)$ describes the degree of coupling, where $\lambda_D$ is the Debye screening length. The plasma is strongly coupled when $\Gamma\gg1$. A rough estimate for the plasmas we are generating ($n_e\approx3\times10^{23}$ cm$^{-3}$ and $T_e\approx50$ eV) yields $\Gamma\approx3.8$ ($\lambda_D\approx1$ Å), and therefore deviations from an ideal plasma might be present. We now consider higher correlation effects which are relevant for strongly coupled plasmas [10] and influence the optical properties in the xuv spectral region. Further theoretical investigations were performed using a refined Drude conductivity model, where the dipole polarizability of the ions [28] and both screening effects and density dependent transport cross sections in the Born and *T*-matrix approximations were taken into account [29,30]. Although only the measured ratio of the harmonics need be used to determine $n_e$ and $T_e$, the relation between the electron density and the refractive index is essential for an interpretation of the results. The refractive index of the harmonics was calculated for a carbon plasma with a temperature of 150 eV and an average degree of ionization of 5.2 as a function of $n_e$ in order to study correlation effects relevant for high densities. This yields a coupling parameter of $\Gamma\approx0.9$ for $n_e=4.5\times10^{23}$ cm$^{-3}$.

The optical properties are determined by the complex dielectric function which is equal to the square of the refractive index $(\eta_r+i\eta_i)^2=\varepsilon(\omega)$. Usually, for a laser-produced plasma, the generalized Lorentz-Drude dielectric function is given by

$$\varepsilon=\varepsilon_{10}+i\varepsilon_{20}-\frac{\omega_p^2}{\omega(\omega+i\nu_{ei})}=\varepsilon_{10}+i\varepsilon_{20}+\frac{i}{\omega\varepsilon_0}\sigma(\omega), \tag{3.1}$$

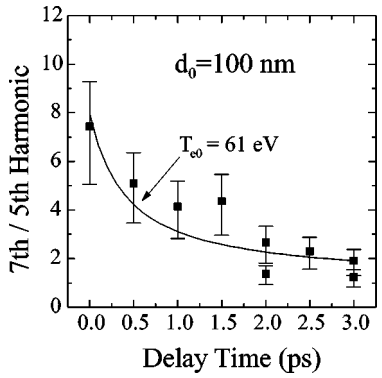


FIG. 12. Measured signal ratio (solid squares) as a function of the delay time deduced from Fig. 11. The curve is a calculation for the time dependence of the ratio assuming $T_{e0}=61$ eV. The curve includes recombination, and is the best fit to the experimental data.

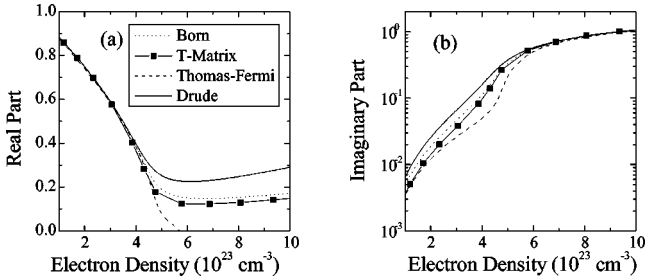


FIG. 13. Real (a) and imaginary (b) parts of the refractive index of a dense carbon plasma as a function of $n_e$ for the fifth harmonic of KrF radiation. Four different calculations were performed for $T_e=150$ eV and a charge state of 5.2. The solid curve represents the result of the standard Drude model, while the dotted curve and square symbols are the results of calculations including high density effects. The dashed curve has been obtained by calculating the refractive index including the ion dipole polarizability effect.

where $\omega_p = \sqrt{n_e e^2/\varepsilon_0 m_e}$ is the local plasma frequency, $\sigma(\omega)$ is the complex conductivity, $\nu_{ei}$ is the electron-ion collision frequency, and $\varepsilon_0$ is the permittivity of free space. The quantities $\varepsilon_{10}$ and $\varepsilon_{20}$ describe the contribution of the bound electrons to the dielectric function which are $\varepsilon_{10}=1$ and $\varepsilon_{20}=0$ for free electron metals or a fully ionized plasma.

When the electron thermal velocity greatly exceeds the maximum oscillatory velocity, the so-called Spitzer-Braginskii formula for the collision frequency can be applied [31]:

$$\nu_{ei} = \frac{4}{3}\sqrt{2\pi}\left(\frac{Ze^2}{4\pi\varepsilon_0 m_e}\right)^2\left(\frac{m_e}{k_B T_e}\right)^{3/2} \times n_i \frac{1}{2}\left(\ln\left[1+\left(\frac{b_{\max}}{b_{\min}}\right)^2\right] + \frac{1}{1+\left(\frac{b_{\max}}{b_{\min}}\right)^2} - 1\right), \tag{3.2}$$

where $Z$ and $n_i$ are the degree of ionization and the ion density, respectively. When the maximum impact parameter $b_{\max}$ greatly exceeds the minimum impact parameter $b_{\min}$, the Coulomb logarithm is usually described by $\ln\Lambda = \ln(b_{\max}/b_{\min})$. In an ideal plasma, $b_{\max}$ is taken to be the Debye screening length, while $b_{\min}$ is given by the impact parameter for perpendicular deflection. This holds only as long as the number of particles in the Debye sphere $N_D = (4\pi/3)\lambda_D^3 n_e$ is large compared to unity. For high densities and low temperatures, the ion sphere radius $\alpha = (3/4\pi n_i)^{1/3}$ was taken as $b_{\max}$.

To improve the standard Drude formula (3.1) with respect to collisions, we start from the relation of the complex conductivity $\sigma(\omega)$ to the dielectric function, which is valid in the long wavelength limit ($\varepsilon_{10}=1,\ \varepsilon_{20}=0$),

$$\varepsilon(\omega) = 1 + \frac{i}{\omega\epsilon_0}\sigma(\omega). \tag{3.3}$$

In the nondegenerate case, the conductivity can be calculated [29,32] from

$$\sigma(\omega) = \frac{e^2 n_e \Lambda_e^3 \hbar^2}{3 m_e^2 k_B T_e}\int \frac{d\vec{k}}{(2\pi)^3}\frac{k^2 \exp[-E_k^e/k_B T_e]}{\nu_{ei}(k) - i\omega}. \tag{3.4}$$

Here $\vec{k}$ is the wave vector of the electron, $E_k^e = \hbar^2 k^2/2m_e$ is the kinetic energy, and $\Lambda_e = \sqrt{2\pi\hbar^2/(m_e k_B T_e)}$ is the thermal wavelength. In contrast to Eq. (3.2) the electron-ion collision frequency is now a function of the wave number, and can be determined from the transport cross section

$$\nu_{ei}(k) = n_i v_e Q^T(k), \tag{3.5}$$

where $v_e$ is the thermal velocity. The cross section can be found analytically in the Born approximation

$$Q^T(k) = \frac{2\pi}{a_0^2 k^4}\left[\ln(1+4k^2\lambda_D^2) - \frac{4k^2\lambda_D^2}{1+4k^2\lambda_D^2}\right], \tag{3.6}$$

where $a_0 = 4\pi\epsilon_0\hbar^2/(Ze^2 m_e)$ is a modified Bohr radius. In the general case of multiple scattering a numerical solution has been obtained ($T$-matrix approximation) [33]:

$$Q^T(k) = \frac{4\pi}{k^2}\sum_{l=0}^{\infty}(l+1)\sin^2[\delta_l(k) - \delta_{l+1}(k)]. \tag{3.7}$$

The $\delta_l$ are phase shifts following from the solution of Schrödinger's equation for the Debye potential $V_D(k) = e^2/(\epsilon_0(k^2+\lambda_D^{-2}))$.

Figures 13 and 14 show the real (a) and imaginary (b) parts of the refractive index for the fifth and seventh harmonics of the KrF wavelength, respectively, as a function of the electron density. The solid curve represents the calculation for the standard Drude formula, while the dotted curve and the squares are the results of the Born and $T$-matrix calculations, respectively, taking improved collision frequencies into account. The dashed curve displays the results of the calculation including ion dipole polarizability. These calculations for the dielectric function were performed with the Thomas-Fermi model to evaluate the charge density distribution inside an ion, and with Bloch's hydrodynamic model [28,34] to account for the coupling between the electrical high frequency field and the plasma. Since no collisions were included in this model, the dashed curve has a singularity at the critical density.

For electron densities below $4\times10^{23}$ cm$^{-3}$ Born, $T$-matrix and ion polarizability calculations show almost no deviation in the real part of the refractive index with respect to the Drude model, while in the imaginary part a discrepancy of up to a factor of 2 appears. At electron densities exceeding $5\times10^{23}$ cm$^{-3}$, one also observes deviations in the real part. However, the standard Drude model has been shown to be a reasonable approximation even for high density plasmas.

The signal of the transmitted fifth and seventh harmonics is now calculated as a function of $n_e$, and is compared to the Drude model which was the basis of the data evaluation [Fig. 15(a)]. The calculations including improved collision frequencies (dotted curve and square symbols) tend to predict a higher transmission than the calculations for an ideal plasma. Consequently, the calculated ratio shown in Fig. 15(b) of the seventh to fifth harmonics versus $n_e$ is shifted toward a higher electron density, which means that for a given measured ratio the inferred electron density is even higher than with the previous analysis. The plasma parameters obtained from the measurement which is presented in Fig. 10 are clos-

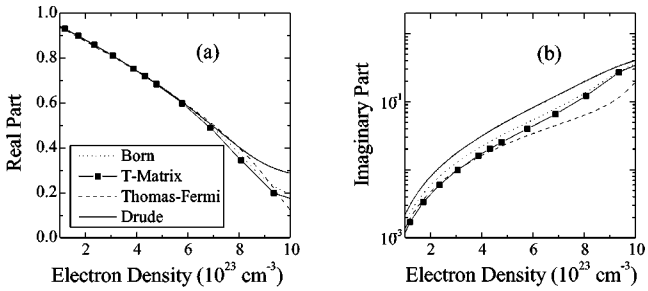


FIG. 14. Real (a) and imaginary (b) parts of the refractive index of a dense carbon plasma as a function of $n_e$ for the seventh harmonic. For these calculations the same conditions as in Fig. 13 are valid.

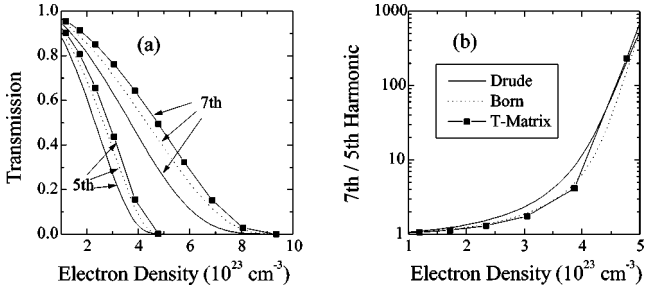


FIG. 15. (a) The calculated behavior of the transmitted fifth and seventh harmonics as a function of $n_e$. The solid curve represents the result obtained from the standard Drude model, while the dotted curve and square symbols are the results of calculations including high density effects. In (b) the ratio of the seventh to the fifth harmonics is displayed vs the electron density.

est to that used for the calculations. Including the improvements an initial electron density of $4.5\times10^{23}$ cm$^{-3}$ is inferred for this measurement, which is 4% higher than previously stated.

## IV. CONCLUSION

A method has been presented to measure both the evolution of the plasma free electron density above $10^{23}$ cm$^{-3}$ and the electron temperature with subpicosecond time resolution. It relies on a pump-probe experimental arrangement, where ultrashort laser produced high harmonics are transmitted through a thin foil plasma which is generated by a separate ultrashort laser pulse. The transmitted harmonic radiation is measured for various delay times, and from the temporal behavior both $n_e$ and $T_e$ are obtained. We have shown that electron densities can be measured to within a precision of 20% for zero delay time. To the best of our knowledge the technique is one of the most precise available in the density range above $10^{23}$ cm$^{-3}$, and in addition has subpicosecond temporal resolution. The interaction of 0.7-ps KrF-laser pulses with thin polycarbonate foils (70–100 nm) at intensities up to $5\times10^{14}$ W/cm$^2$ resulted in electron densities of up to $(4.3^{+0.6}_{-0.8})\times10^{23}$ cm$^{-3}$ and electron temperatures of up to $(122^{+92}_{-56})$ eV. Theoretical studies of the optical properties of a carbon plasma in the xuv range showed that density effects in the real part of the refractive index become important for densities above $5\times10^{23}$ cm$^{-3}$. The imaginary part of the refractive index in the density range from $1\times10^{23}$ cm$^{-3}$ to $1\times10^{24}$ cm$^{-3}$ is slightly overestimated by the Drude model when compared to theories including correlation effects, relevant for high density plasmas. The method described here will give valuable information of plasma parameters relevant for experiments in the fields of inertial confinement fusion, and x-ray laser development, and in general for the investigation of high density strongly coupled laser-produced plasmas.

## ACKNOWLEDGMENTS

The authors would like to thank B. U. Felderhof for valuable discussions, and for a critical reading of the manuscript. We also would like to thank P. Gibbon for his help with the MEDUSA code. This work was supported by the European Community in the network ''Super Intense Laser Solid Interaction'' under Contract No. ERB4061 PL 95-0765, and by the Deutsche Forschungsgemeinschaft under Contract No. TH 700/1-1.

## APPENDIX: REFRACTION OF HARMONICS

In this appendix, refraction of harmonics in a steep lateral density gradient is calculated. For an intermediate scale length refraction must be taken into account which is treated here in the approximation of geometrical optics [35],

$$\frac{1}{R(\vec{r})}=\hat{N}\frac{\vec{\nabla}\eta(\vec{r})}{\eta(\vec{r})}, \tag{A1}$$

where $R(\vec{r})$ is the radius of curvature of the rays that are bent in a locally changing refractive index $\eta(\vec{r})$, and $\hat{N}$ is a unit vector in the direction of the tangent of the ray path. We consider only a change in the radial component of the refractive index assuming cylindrical symmetry with the $z$ direction as the direction of the incident beam. Equation (A1) can then be rewritten as

$$\frac{1}{R(r,\alpha)}=\cos(\alpha)\frac{d\eta(r)/dr}{\eta(r)}, \tag{A2}$$

where $\alpha$ is the angle between $\hat{N}$ and the refractive index gradient. The radiation that passes through the foil plasma is

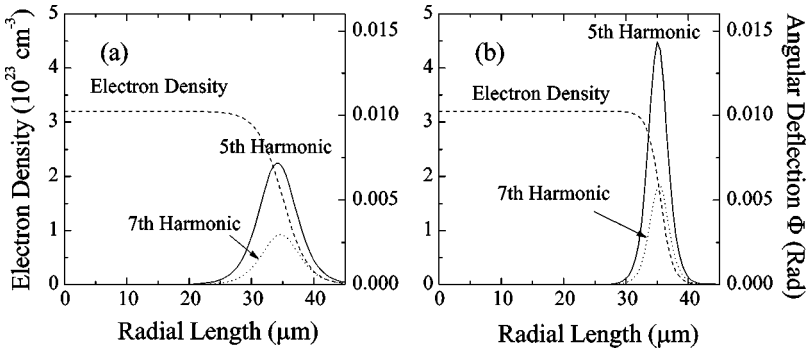


FIG. 16. Calculation of the refraction of the fifth (solid curve) and seventh (dotted curve) harmonics for a lateral electron density profile (dashed curve) with a softened flat-top-like distribution and a maximum of $n_e=3.2\times10^{23}$ cm$^{-3}$. In (a) a radial scale length of 8.8 $\mu$m is assumed, which is defined as the length over which the density drops from 90% to 10% of the maximum. In (b) a scale length of 4.4 $\mu$m is assumed, resulting in a stronger deflection of both harmonics. The half collection angle of the spectrograph is 8 mrad, and therefore part of the fifth harmonic that is incident in the range of the steepest density gradient will be lost.

deflected with an angle $\Phi$, which depends on the electron density profile and the thickness of the plasma slab.

Figure 16 shows a calculation of the total angular deflection $\Phi$ (see Fig. 9) for a 100-nm-thick foil plasma with a radial flat-top-like density profile and a maximum electron density of $n_e = 3.2 \times 10^{23}$ cm$^{-3}$. Figure 16(a) shows the calculation for a radial scale length of 8.8 $\mu$m, and Fig. 16(b) that for a scale length of 4.4 $\mu$m. The radial scale length is defined here as the length over which the density drops from 90% to 10% of the maximum. The refraction of the fifth harmonic is stronger than that of the seventh harmonic, as expected, but in case (a) the whole signal of both transmitted harmonics will still be collected by the spectrograph with a half collection angle of 8 mrad. In Figure 16(b) part of the fifth harmonic is so strongly deflected that it is out of the acceptance angle of the spectrograph, and hence the measured ratio of the seventh to the fifth harmonics, $R_{7/5}$, will be slightly higher than without refraction. Hence, from the measured ratio $n_e$ tends to be overestimated. A correction of $R_{7/5}$ with respect to refraction is not possible, since the exact values of the scale length and the shape of the electron density profile are not known. However, an estimate of the effect will be given in order to cover this uncertainty. Suppose refraction losses diminishes the measured signal of the harmonics by a factor of $x_5$ and $x_7$, respectively. In this case $R_{7/5}$, including refractive losses, will be

$$R_{7/5} = \frac{H_{7,\mathrm{trans}} - H_{7,\mathrm{refr}}}{H_{5,\mathrm{trans}} - H_{5,\mathrm{refr}}} = \frac{H_{7,\mathrm{trans}}(1-x_7)}{H_{5,\mathrm{trans}}(1-x_5)}. \tag{A3}$$

It is assumed that the refraction and absorption are independent processes, and that the detected signal is linearly diminished due to refraction losses. The measured ratio (without refractive corrections) must be divided by the factor $(1-x_7)/(1-x_5)$ in order to calculate the correct value for $n_e$.


[1] M. M. Murnane, H. C. Kapteyn, and R. W. Falcone, Phys. Rev. Lett. **62**, 155 (1989).

[2] H. M. Milchberg, R. R. Freeman, S. C. Davey, and R. M. More, Phys. Rev. Lett. **61**, 2364 (1988).

[3] J. C. Kieffer, Z. Jiang, A. Ikhlef, C. Y. Cote, and O. Peyrusse, J. Opt. Soc. Am. B **13**, 132 (1996).

[4] J. Workman, A. Maksimchuk, X. Liu, U. Ellenberger, J. S. Coe, C. Y. Chien, and D. Umstadter, Phys. Rev. Lett. **75**, 2324 (1995).

[5] U. Teubner, J. Bergmann, B. van Wonterghem, F. P. Schäfer, and R. Sauerbrey, Phys. Rev. Lett. **70**, 794 (1993).

[6] R. Fedosejevs, R. Ottman, R. Sigel, G. Kühnle, S. Szatmari, and F. P. Schäfer, Appl. Phys. B: Photophys. Laser Chem. **50**, 79 (1990).

[7] D. F. Price, R. M. More, R. S. Walling, G. Guethlein, R. L. Shepherd, R. E. Stewart, and W. E. White, Phys. Rev. Lett. **75**, 252 (1995).

[8] U. Teubner, I. Uschmann, P. Gibbon, D. Altenbernd, E. Förster, T. Feurer, W. Theobald, R. Sauerbrey, G. Hirst, M. H. Key, J. Lister, and D. Neely, Phys. Rev. E **54**, 4167 (1996).

[9] T. Feurer, W. Theobald, R. Sauerbrey, I. Uschmann, D. Altenbernd, U. Teubner, P. Gibbon, E. Förster, G. Malka, and J. L. Miquel, Phys. Rev. E **56**, 4608 (1997).

[10] W. D. Kraeft, D. Kremp, W. Ebeling, and G. Röpke, *Quantum Statistics of Charged Particle Systems* (Plenum, New York, 1986).

[11] W. Theobald, R. Häßner, R. Kingham, T. Feurer, H. Schillinger, G. Schäfer, and R. Sauerbrey, in *Proceedings of Ultrafast Phenomena XI*, edited by T. Elsaesser, J. G. Fujimoto, D. A. Wiersma, and W. Zinth, Springer Series in Chemical Physics (Springer, Berlin, 1998), pp. 410ff.

[12] B. A. Remington, J. Kane, R. P. Drake, S. G. Glendinning, K. Estabrook, R. London, J. Castor, R. J. Wallace, D. Arnett, E. Liang, R. McCray, A. Rubenchik, and B. Fryxell, Phys. Plasmas **4**, 1994 (1997).

[13] W. Theobald, R. Häßner, C. Wülker, and R. Sauerbrey, Phys. Rev. Lett. **77**, 298 (1996).

[14] A. L'Huillier and Ph. Balcou, Phys. Rev. Lett. **70**, 774 (1993).

[15] S. Szatmári and F. P. Schäfer, Opt. Commun. **68**, 196 (1988).

[16] G. Almàsi, S. Szatmári, and P. Simon, Opt. Commun. **88**, 231 (1992).

[17] J. Peatross and D. D. Meyerhofer, Phys. Rev. A **51**, R906 (1995).

[18] S. P. Le Blanc, Z. Qi, and R. Sauerbrey, Opt. Lett. **20**, 312 (1995).

[19] F. R. Powell, P. W. Vedder, J. F. Lindblom, and S. F. Powell, Opt. Eng. (Bellingham) **29**, 614 (1990).

[20] J. Jasny, U. Teubner, W. Theobald, C. Wülker, J. Bergmann, and F. P. Schäfer, Rev. Sci. Instrum. **65**, 1631 (1994).

[21] J. C. Gauthier, in *Laser-Plasma Interactions 4*, edited by M. B. Hooper (SUSSP Publications, Edinburgh, 1988).

[22] H. R. Griem, *Plasma Spectroscopy* (McGraw Hill, New York, 1964), p. 139.

[23] R. F. Reilman, and S. T. Manson, Astrophys. J., Suppl. **40**, 815 (1979).

[24] D. E. Osterbrock, *Astrophysics of Gaseous Nebulae and Active Galactic Nuclei* (University Science Books, Mill Valley, CA, 1989).

[25] B.-T. V. Vu, A. Szoke, and O. L. Landen, Phys. Rev. Lett. **72**, 3823 (1994).

[26] J. P. Christiansen, D. E. T. F. Ashby, and K. V. Roberts, Comput. Phys. Commun. **7**, 271 (1974).

[27] A. Djaoui and S. J. Rose, J. Phys. B **25**, 2745 (1992).

[28] K. Ishikawa and U. B. Felderhof, J. Plasma Phys. (to be published).

[29] G. Röpke, C. V. Meister, K. Kollmorgen, and W. D. Kraeft, Ann. Phys. (Leipzig) **36**, 377 (1979).

[30] F. Morales, K. Kilimann, R. Redmer, M. Schlanges, and F. Bialas, Contrib. Plasma Phys. **29**, 425 (1989).

[31] P. Mulser, in *Laser Solid Interactions with Atoms, Solids, and Plasmas*, Vol. 327 of *NATO Advanced Study Institute Series B: Physics*, edited by R. M. More (Plenum, New York, 1994).

[32] W. D. Kraeft, J. Blümlein, and Th. Meyer, Contrib. Plasma Phys. **23**, 9 (1983).

[33] D. O. Gericke, M. Schlanges, and W. D. Kraeft, Laser Part. Beams **15**, 523 (1997).

[34] F. Bloch, Z. Phys. **81**, 363 (1933).

[35] M. Born and E. Wolf, *Principles of Optics*, 6th ed. (Pergamon, Oxford, 1993).